LAWRENCE
LIVERMORE
NATIONAL
LABORATORY

UCRL-CONF-233411

Generic thermo-mechanical model for jointed rock masses

Oleg Vorobiev

August 7, 2007

PLasticity 2007
Anchorage, AK, United States
June 1, 2007 through June 6, 2007

Generic thermo-mechanical model for jointed rock masses

Oleg Vorobiev

Lawrence Livermore National Laboratory

L-206,P.O. Box 808, 7000 East Avenue, Livermore, CA 94551

vorobiev1@llnl.gov

Abstract

A new nonlinear thermo-mechanical model for heavily jointed rock masses is presented. The model describes poroelasticity, shear-enhaced compaction and brittle-ductile transition in porous dry rocks. The basic input parameters in the model such as elastic moduli, tensile and compressive strength are expressed as functions of the reference porosity of the rock. These functions are based on empirical data for some types of rocks (limestones, sandstones). The model assumes that the media is isotropic. Effects of joints is modelled by scaling down the key model parameters. The scaling rules rely on empirical data but can also be found from direct comparison with the explicit simulation of jointed rock masses

Keywords: geological material, rock, constitutive behaviour, yield condition, plastic collapse

1. Introduction

Modeling thermo-mechanical response of jointed rock presents a challenge even for small deformations. This is because both the joints and the rock may exhibit strongly non-linear mechanical response, anisotropy and rate dependence. Large-scale in situ tests are expensive and in some cases not possible. In Situ tests generally provide information on P-wave and S-wave velocities as well as the joint spacing but not on the failure surface for the confined rock masses.

Therefore numerical modeling is an important tool to study and analise the response of the jointed rock masses. The presence of joints and cracks makes the response scale dependent. This means that the effective mechanical properties of the media will depend on the size of the problem. One of the key questions is how to scale these properties from the lab sample size to the inSitu one. In the present study we apply explicit models for the joints to derive these scaling rules for the homogenized model of the jointed media. There are different methods to model jointed media. One of the most popular method used in rock mechanics is the DEM where the blocks of the rock and joints are modeled separately (Cundall [1992]). The DEM approach is very expensive computationally but can be used to calibrate phemenological continuum models for in situ blocky rock masses. The advantage of DEM methods is that it can deal with large deformations of the rock masses (block separation,splitting etc) in a natural way. The disadvantages of DEM methods include difficulties in modeling nonpersistent joints and cracks. Alternative methods to model discontinuos media include the discrete-continuum approach Lin [2006], XFEM (Belytschko et al [2007]) where the finite elements containing the joints are treated in a special way, the thin elements used to model joints (Desai [1984];Wang [2003]), and numerous analitical methods developed in assumption of linear elastic media (Gerrard [1982];Fossum [1985];Cai [1992]).

In the present work we intend to study rock response at high confinements where both the joints and the material show strongly nonlinear behaviour and large deformation. Therefore using contact algorithms such as simple common plane (Vorobiev [2007]) seems to be a more robust method compared to the schemes employing connected elements.

For large scale simulations it is not practical to count every single joint in the problem explicitly. When the wave length is much bigger than the joint spacing it may be appropriate to use homogenization techniques to derive equivalent properties for the rock mass. The basis of the homogenized inSitu model is the model based on isotropic plasticity theory (Vorobiev O. Yu., Liu B.T. et al [2007]) which describes triaxial tests for the intact rock samples. It is known that the rock properties may vary significantly from sample to sample. Therefore it is important to

parametrize the key model parameters such as Unconfined Compressive Strength (UCS), the initial bulk modulus, the crush pressure in order to capture this variability. One example of such parametrization is given in Aubertin [2004] where the yield surface is scaled down with increased porosity. In the current model not only the yield surface but also the elastic moduli depend on the reference porosity of the rock. To extend the model from the intact sample scale to the inSitu scale one can use empirical rules such as (Hoek and Brown [1998]) or find the scaling rules from the direct explicit simulation of the jointed media. In rock mechanics it is common to use rock mass characterization indices such as GSI,RMS etc based on visual observations. Empirical failure surfaces are often expressed in terms of these indices. However, most of these criteria do not address postfailure behaviour and are used for quasistatic problems of rock engineering. Recently attempts were made to extend the GSI qualification system to the residual strength of rocks (Cai [2007];Tiwari [2006]). The current approach offers an option to rely on these empirical scaling rules as first order estimates when homogenized model is used for the large scale calculations.

Equivalent continuum approach is widely used in practical analisys of heavily jointed rock masses. In some codes depending on the joint number and orientation different effective mechanical properties can be calculated within each finite element. Most of these models assume that the element size should be bigger than some Representative Volume Element (REV) (Cai [1992]). But some (Pariseau [1999];Zhu [1993]) can handle individual joints as well. The NRVE(non-representative volume element approach (Pariseau [1999]) keeps track of the local strains for all materials within the element and calculates average stresses using so called ``strain influence matrix" describing partitioning of deformations amoung the materials. In both NRVE and REV methods mentioned above the rocks and joints are generally represented by linear elastic materials and thus can be only applied for small deformations.

The objective of this paper is to develop a methodology to model nonlinear dynamic response for in situ rock masses. The in situ model is build as an extension of the model for intact

rock samples (Vorobiev O. Yu., Liu B.T. et al [2007]) with scaled down strength and elastic properties. The scaling can be done according to the Hoek-Brown empirical rule using GSI index characterizing the rock mass quality. The model is designed for wide range of loads from quasi-static triaxial test modeling to the shock wave loading. Continuum model is compared with explicitly modeled jointed media where the joints are modeled using advanced contact detection described in Vorobiev [2007]. This comparison allows us to study the correlation between effective elastic moduli and the strength of the rock masses for a wide range of loading conditions.

2. Model for intact material

2.1. Basic equations

The thermomechanical structure of the model is based on the developments in (Rubin et al [1996];Rubin et al [2000]). Within this context, an elemental volume dv of the porous material in the present configuration expresses as the sum of solid volume and pore volume , such that

$$dv = dv_s + dv_p, \qquad dV = dV_s + dV_p, \tag{1}$$

where $\{dV, dV_s, dV_p\}$ are the values of $\{dv, dv_s, dv_p\}$, respectively, in a fixed reference configuration. The porosity ϕ and its reference value Φ are defined by

$$\phi = \frac{dv_p}{dv}, \qquad \Phi = \frac{dV_p}{dV} \tag{2}$$

The total dilatation, J, and the average dilatation of the solid, J_s, are defined by

$$J = \frac{dv}{dV}, \qquad J_s = \frac{dv_s}{dV_s} = \left(\frac{1-\phi}{1-\Phi}\right) J \tag{3}$$

The elastic response of the solid is characterized by the dilatation, J_s, in Eq.(3) where

the total dilatation, J, is determined by the evolution equation

$$\frac{\dot{J}}{J} = \mathbf{D} \bullet \mathbf{I}, \qquad \mathbf{D} = \frac{1}{2}\left(\mathbf{L} + \mathbf{L}^{\mathrm{T}}\right) \tag{4}$$

A symmetric unimodular tensor $\mathbf{B}_{\mathbf{e}'}$ is used as a measure of pure elastic distortion in the evolution equation

$$\dot{\mathbf{B}}_{\mathbf{e}}' = \mathbf{L}\mathbf{B}_{\mathbf{e}}' + \mathbf{B}_{\mathbf{e}}'\mathbf{L}^{\mathrm{T}} - \frac{2}{3}(\mathbf{D} \bullet \mathbf{I})\mathbf{B}_{\mathbf{e}}' - \mathbf{A}_{\mathbf{p}}, \mathbf{A}_{\mathbf{p}} = \Gamma_p\left(\mathbf{B}_{\mathbf{e}}' - \left(\frac{3}{\mathbf{B}_{\mathbf{e}}'^{-1} \bullet \mathbf{I}}\right)\right), \tag{5}$$

where the tensor, $\mathbf{A}_{\mathbf{p}}$, characterizes the direction and magnitude of inelasticity for distortional response and Γ_p requires an additional constitutive equation, (see Rubin [2000] for example.)

In contrast to many other purely mechanical models used for rocks and geologic materials (see for example, Fossum [2004];Shao [1991];Xie [2006]) the current model is a thermo-mechanical one. It is derived from the assumption that the Helmholtz free energy Ψ is a function of the variables J_s, an invariant $\alpha_1 = \mathbf{B}_{\mathbf{e}}' \bullet \mathbf{I}$ of $\mathbf{B}_{\mathbf{e}'}$ and temperature Θ:

$$\rho_{s0}\Psi_s(J_s, \Theta, \alpha_1) = \rho_{s0}\hat{\Psi}(J_s, \Theta) + \frac{1}{2}G(J_s, \Theta)(\alpha_1 - 3) \tag{6}$$

If we neglect a small terms in pressure related to α_1 then the stress tensor $\mathbf{T}$ can be expressed as:

$$\mathbf{T} = -p\mathbf{I} + \mathbf{T}', \quad p = (1 - \phi - J\frac{\partial \phi}{\partial J})p_s, p_s = -\rho_{s0}\frac{\partial \Psi}{\partial J_s}, \quad \mathbf{T}_{\mathbf{s}'} = J_s^{-1}G(J_s, \Theta)\mathbf{B}_{\mathbf{e}''}, \tag{7}$$

where p is the pressure, $\mathbf{T}'$ is the deviatoric part of the stress, $\mathbf{B}_{\mathbf{e}}''$ is the deviatoric part of $\mathbf{B}_{\mathbf{e}}'$ and p_s and $\mathbf{T}_{\mathbf{s}'}$ are the pressure and deviatoric stress of the solid matrix, respectively. The solid pressure can be defined,for example,with Mie-Gruneisen equation of state as

$$p_s = p_c(\rho_s) + \gamma \rho_{s0} \varepsilon \tag{8}$$

The reference curve $p_c(\rho_s)$ is derived from shock experiments or approximations of the cold curve, ε is specific internal energy and γ is Gruneisen coefficient.

2.2. Elastic properties and poroelasticity

Experimental data on hydrostatic compression of porous rocks show nonlinear elastic response up to 10-100 MPa (Vajdova [2004]). This response can be attributed to the elastic closing of the microcracks. To model such nonlinear response we introduce poroelasticity effect by expressing the porosity as a function of J and a history dependent unloaded porosity ϕ_u as

$$\phi = \phi_u \frac{x}{(1+x)}, x = \frac{a(\Phi)(1-\phi_u)(J_u/J-1)}{\phi_u}, J_u = \frac{1-\Phi}{1-\phi}, a(\Phi) = min(1, a_0\sqrt{\Phi}), \tag{9}$$

where a_0 is the material constant. The unloaded porosity ϕ_u describes the porosity that would exist if the material was unloaded from the current state. This formulation provides right asymptotic behavior and can be shown to satisfy the second law of thermodynamics if coupled with the evolution equations for ϕ_u described later. Compared with the function used in Rubin [1996], the advantage of Eq.(9) is that it allows to calculate unloaded porosity at given porosity and compression analytically. Using Eq.(7) and Eq.(9) the bulk modulus can be written as

$$K = -J\frac{\partial p}{\partial J} = K_s(1-\phi_u)\left(1 - \frac{a(\Phi)J_u}{J(1+x)^2}\right)^2 - \frac{2a(\Phi)^2(1-\phi_u)^2 J_u^2}{J^2\phi_u(1+x)^3} p_s \tag{10}$$

In unloaded state, where $p_s \to 0, x \to 0, J_u/J \to 1$, the initial bulk modulus K_0 is equal to a fraction of the solid modulus K_s as

$$K_0 \to K_s(1-\Phi)(1-a(\Phi))^2, \quad K_s = -J_s \frac{\partial P_s}{\partial J_s} \tag{11}$$

Initial bulk modulus shows a good correlation with the porosity of the rock. Experimental data from Vajdova [2004] are shown in **Figure 1** together with the model calculations using Eq (11).

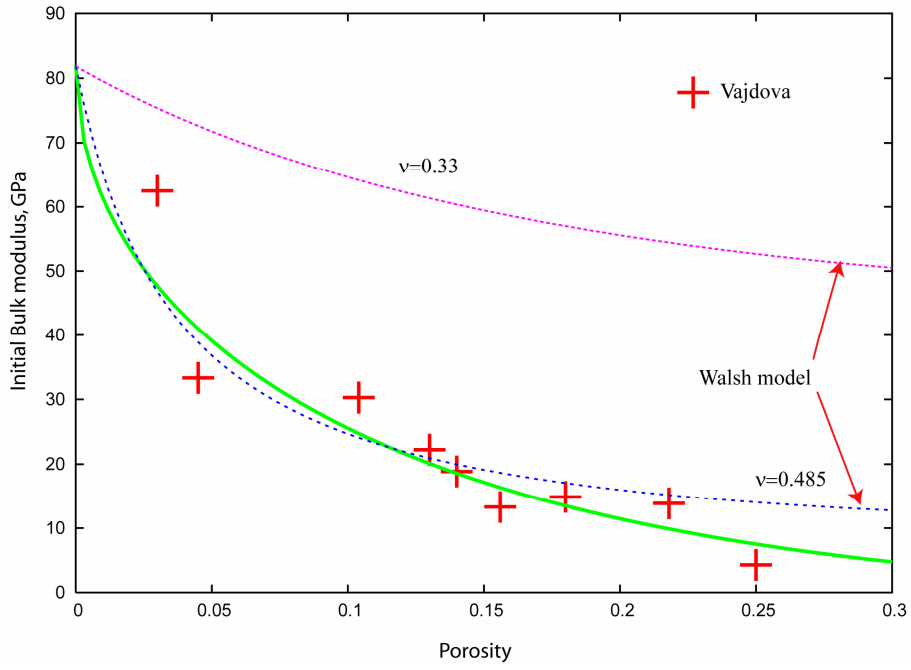

Figure 1 Porosity - initial bulk modulus correlation for the limestones. The solid line is the results for the current model, the dashed lines are predictions with Walsh model (Walsh [1965]) using two different Poisson ratios.

Bulk modulus reduction with porosity can be explained with a simple model (Walsh

[1965]) considering an elastic matrix embedded with spherical pores. According to that model effective compressibility of the rock is expressed as

$$\frac{1}{K_0} = \frac{1}{K_s}\left(1 + \frac{3(1-\nu)\Phi}{2(1-2\nu)(1-\Phi)}\right), \tag{12}$$

where ν is the Poisson ratio.

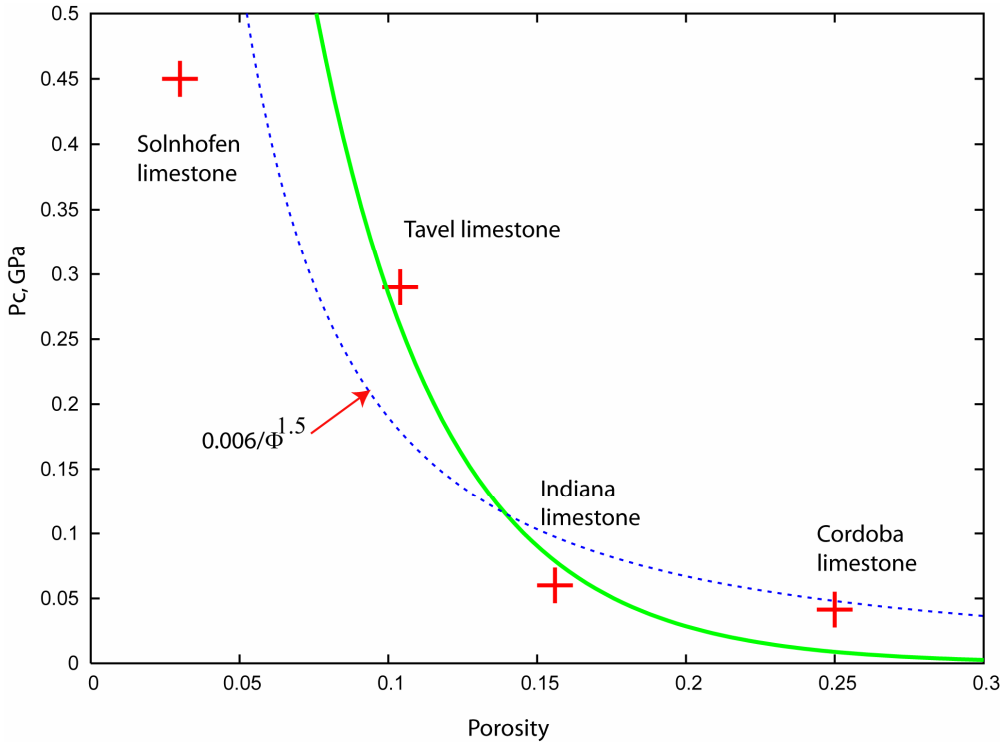

Figure 2 Porosity - crush pressure correlation for the limestones.

The initial value of the crush pressure, P_c depends on the porosity as well as the grain size. Hertzian fracture model relates the onset of the grain crushing with the porosity as

$$P_c = 2.2\frac{(1-\nu^2)^2 K_{IC}^3}{E^2(1-2\nu)^3(\Phi c)^{3/2}}, \tag{13}$$

where c is the length of preexisting crack and K_{IC} is the fracture toughness coefficient. It is reasonable to assume that the crack length c in Eq.(13) is proportional to the grain size. This explains the observed dependence of P_c on the product of the grain size and porosity for the limestones (Vajdova [2004]) and the sandstones (Wong [1997]).

Information on grain size is not easily available but very often low-porosity samples have smaller grain size than more porous ones. Therefore it is reasonable to use porosity correlation for P_c.

Figure 2 shows the correlation between the porosity of the limestone samples and the value of P_c measured in hydrostatic compression tests. It is interesting to note that since both P_c and the initial bulk modulus K_0 decrease with porosity, the strain to compaction, μ_c, defined as $\mu_c = \frac{P_c}{K_0}$ may not be sensitive to the porosity. For example, for the limestones with 7.5-15% porosity $\mu_c = 0.01 \pm 0.001$. Therefore the current model uses $\mu_c(\Phi)$ correlation function for the input.

2.3. Yield Surface

The current model introduces three pressure dependent surfaces that govern the material response during yielding: the initial yield surface (onset of yield), $Y_0(p)$, the failure surface, $Y_f(p)$, and the residual surface $Y_r(p)$ (see Figure 3).

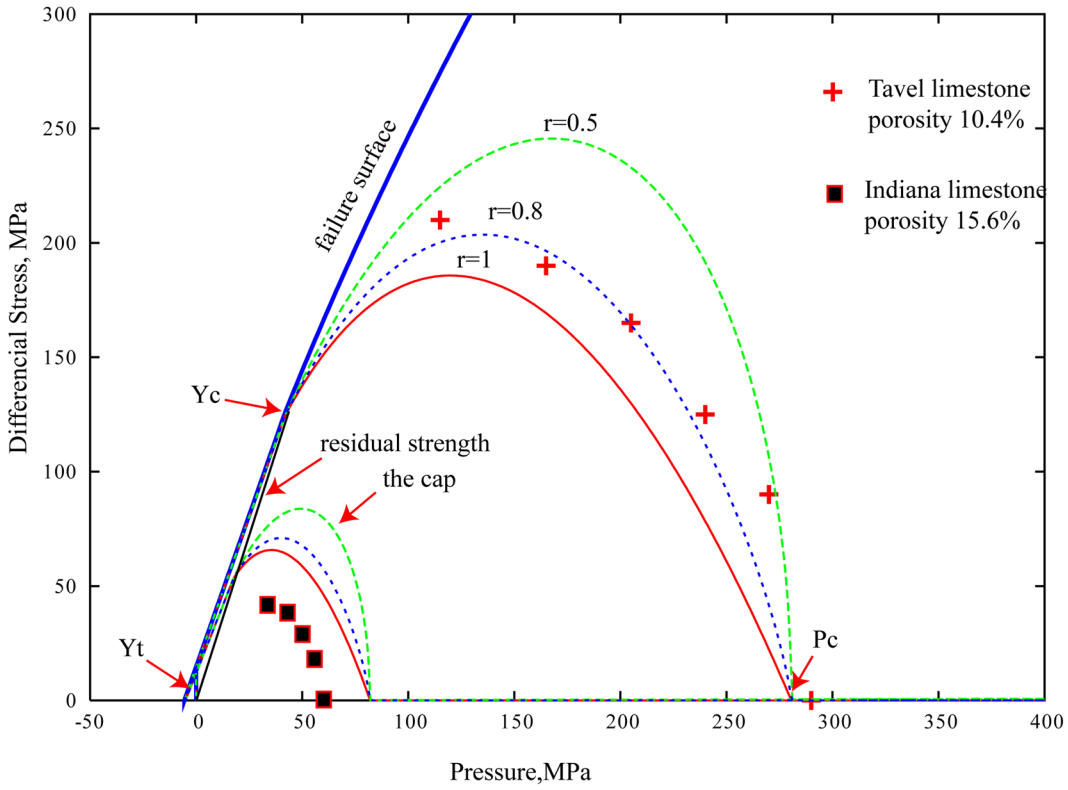

Figure 3. Yield surfaces in Y-P plane. The cap is calculated for three different values of r parameter. The pressure corresponding to the beginning of compaction in hydrostatic conditions $P_c(\Phi)$ is defined by the compaction curve.

The yield strength corresponding to a generalized triaxial compression state, Y_{TXC}, is derived from Y_0, Y_f, and Y_r such that

$$Y_{TXC}(p) = \left(\delta_h Y_f(p) + (1-\delta_h) Y_0(p)\right)(1-\Omega) + \Omega Y_r(p) \tag{14}$$

The equivalent plastic strain ε_p, determined by integrating the following evolution equation

$$\dot{\varepsilon}_p = \left(\frac{2}{3}\mathbf{D_p} \bullet \mathbf{D_p}\right)^{1/2}, \mathbf{D_p} = \frac{1}{2}\Gamma_p \mathbf{A_p} \approx \frac{1}{2}\Gamma_p \mathbf{B_{e''}}, \tag{15}$$

is used to define a hardening parameter δ_h as

$$\delta_h = \frac{\varepsilon_p}{\varepsilon_p + \varepsilon_{hard}}, \tag{16}$$

where ε_{hard} is a constant.

We use a measure of damage, Ω expressed through the history variable ϕ_2, the total amount of bulking porosity (dilatancy) generated in the material, as

$$\Omega = \frac{\langle \phi_2 - \phi_{cr} \rangle D}{1 + \langle \phi_2 - \phi_{cr} \rangle D}, 0 \le \Omega \le 1, \tag{17}$$

where D is the rate of softening and ϕ_{cr} is a threshold value of porosity. As damage accumulates during loading, the material softens and its strength approaches the residual curve

$$Y_r(p) = min\{Y_0(p), Y_0(P_0)\frac{p}{P_0}\} \tag{18}$$

The initial yield surface is expressed in the form

$$Y_0(p) = CY_f(p)\left[\frac{1 - p/P_c}{1 - \xi(\Phi)}\right]^r, 0 \le C \le 1, \tag{19}$$

where C and r are constants.Compaction pressure $P_c(\Phi, J)$ changes as porosity is compacted.

Model parameter r controls the shape of the cap. Figure 3 shows three initial yield surfaces calculated with r=0.5, r=0.8 and r=1 as well as experimental initial yield points for Indiana and Tavel limestones. The values $r \le 0.5$ give the cap with an infinite slope at $P = P_{c0}$,

where P_{c0} is the pressure corresponding to the onset of compaction.

Function $\xi(\Phi)$ is defined as

$$\xi(\Phi) = \frac{P_{BD}}{P_{c0}} = \frac{Y_c(\Phi) R_{BD}(\Phi)}{\mu_c(\Phi) K_0(\Phi)} \tag{20}$$

where $R_{BD}(\Phi)$ is the ratio of the brittle-ductile transition pressure to the unconfined compressive strength. If no data available for R_{BD} it can be estimated from the intersection of Mogi line (Mogi [1974]) with the onset curve $CY_f(p)$.

The ultimate strength function, $Y_f(p)$ is based on the H&B strength criterion (Hoek and Brown [1998]) that relates the maximum (σ_1) and minimum (σ_3) principal stress on the failure surface as

$$\sigma_1 = \sigma_3 + Y_c \left(m \frac{\sigma_3}{Y_c} + s \right)^n \tag{21}$$

For most rocks $\frac{1}{2}$ is a reasonable value for n. Parameter s is equal to unity for intact material and less than unity for in situ material. Hoek [1998] gives an empirical relationship between the coefficients, s and m and the Geologic Strength Index (GSI)

$$s = exp\left(\frac{GSI - 100}{9} \right), m = m_i exp\left(\frac{GSI - 100}{28} \right) \tag{22}$$

In Eq(22), m_i is the value of m for intact rock; it can be obtained from static lab tests.

For triaxial compression with $\sigma_e = Y_f$, the principal stresses σ_1 and σ_3 are given by

$$\sigma_1 - \sigma_3 = Y_f, \quad \sigma_3 = p - \frac{Y_f}{3}, \tag{23}$$

so that the H&B function (12) yields

$$\frac{Y_f}{Y_c} = \left(s + \frac{mp}{Y_c} - \frac{mY_f}{3Y_c} \right)^n \tag{24}$$

When n=0.5, Eq.(23) becomes a quadratic equation and the failure strength Y_f can be expressed in terms of pressure and unconfined compressive strength Y_c as

$$Y_f = Y_c \sqrt{s + \frac{m^2}{36} + \frac{mp}{Y_c}} - \frac{m}{6} \tag{25)(26}$$

Equation(26) may not be flexible enough to describe uniaxial strength both in compression and tension. Therefore the following, more general function is used

$$Y_f(p) = \begin{cases} Y_{f1}(p) & p > Y_c/3 \\ Y_{f2}(p) & p \le Y_c/3 \end{cases}$$

where functions Y_{f1} and Y_{f2} are expressed as

$$Y_{f1}(p) = Y_c \left(s + \frac{m^2}{36} + \frac{mp}{Y_c} \right)^n + s^n - \left(s + \frac{m^2}{36} + \frac{m}{3} \right)^n, \tag{27}$$

$$Y_{f2}(p) = \frac{p/Y_c + s\beta}{1/3 + \beta}, \beta = \frac{2R_t}{3(1-R_t)}, R_t = Y_t/Y_c \tag{28}$$

For the inSitu material the value of unconfined compressive strength is

$$Y_c^{inSitu} = Y_c SRF \tag{29}$$

where the strength reduction factor, SRF, is $SRF = s^n$. The value of Y_c for the intact material can be found from unconfined compressive tests. According to ``sliding wing crack theory" it can be expressed as

$$Y_c = \frac{\sqrt{6}}{\sqrt{1+\mu^2} - \mu} \frac{K_{IC}}{\sqrt{\pi c}} \tag{30}$$

where c is the average length of preexisting cracks (Baud [2000]). It is reasonable to assume that c is of the order of the average grain size. Generally, less porous rocks have smaller grain size, so the value of Y_c decreases with porosity for the same type of rocks. Beside the grain size the strength of sedimentary rocks has been found to depend on other factors such as the amount of calcite, the texture, pores distribution (Torok [2006]). This means that for each data set one should use a specific correlation which takes these factors into consideration. Review of empirical correlations between strength and porosity can be found in Chang [2006].

Figure 4 shows the exponential correlation function used in the model and some experimental points.

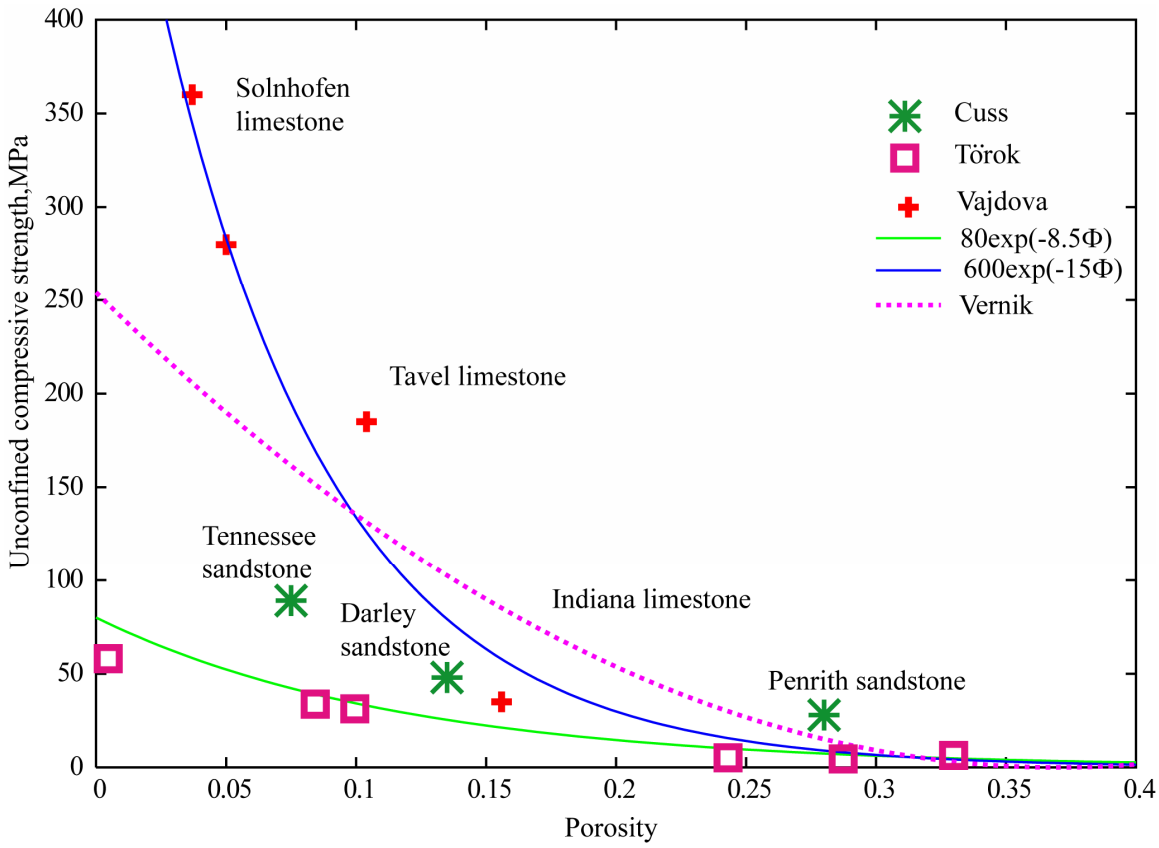

Figure 4. Correlation between Yc and the reference porosity for various sedimentary rocks. The points are the experimental data (Vajdova [2004];Torok [2006]), the solid lines are exponential fits to two different sets of data for the limestones, the dashed line is the empirical correlation used for the sandstones (Vernik [1993]) and the stars are the data for various sandstones (Cuss [2003])

The final yield surface including loading direction effects takes the form

$$Y = Y_{TXC}(p)F(\beta) \tag{31}$$

where $F(\beta)$ is a function of the lode angle described in Rubin et al[2000].

2.4. Porous compaction and dilation

The evolution equation for the unloaded porosity ϕ_u is similar to one described in (Vorobiev O. Yu., Liu B.T. et al [2007]). For simplicity, we assume that there is no rate dependence. The unloaded porosity is found as

$$\phi_u = \Phi - S(\Phi)(1-\Phi)\langle 1/J - \mu_e + \mu_s - \mu_b - \mu_c(\Phi)\rangle \tag{32}$$

The shifts μ_b, μ_s, μ_e model effects of bulking, shear enhanced compaction and heating. The value of μ_e can be found be inverting EOS as

$$\mu_e = \varepsilon/\left((1-\Phi)\partial p_s/\partial \rho_s\right) \tag{33}$$

The bulking shift μ_b is proportional to the amount of produced bulking porosity as

$$\mu_b = \frac{\bar{\gamma}\phi_2}{S(\Phi)(1-\Phi)} \tag{34}$$

The bulking porosity ϕ_2 is a history variable decribing extra porosity produced due to dilatancy for all times using the following equation:

$$\dot{\phi}_2 = \frac{A_0 + A_1\langle dY/dp\rangle}{1+\langle dY/dp\rangle}\langle dY/dp\rangle\dot{\varepsilon}_p(1-\phi) \tag{35}$$

Because the rate of bulking is proportional to the positive slope of the yield surface, the dilatancy and the brittle response take place only at low confinements where the cap is not applied.

The shear-enhanced compaction shift is expressed as

$$\mu_s = \frac{P_c(\Phi)}{K}(1-\xi)\left(\frac{\sigma_e}{CY_f(p)}\right)^{1/r} \tag{36}$$

where σ_e is the current Von Mises Stress, K is the current bulk modulus and P_c is the current compaction pressure found as

$$P_c(\Phi) = p + K\left(\frac{\Phi-\phi}{S(\Phi)(1-\phi)} + \mu_c(\Phi) + \mu_e + \mu_b - 1/J\right) \tag{37}$$

The rate of compaction is defined by the slope S which in turn depends on the amount of the shear-enhanced compaction shift, μ_s, as

$$S(\Phi) = \frac{\Phi S_0(\Phi)}{\Phi + \mu_s S_0(\Phi)(1-\Phi)} \tag{38}$$

where $S_0(\Phi)$ is the compaction slope for hydrostatic condition defined as a function of the reference porosity. The function $S_0(\Phi)$ is fitted by modeling hydrostatic compressions of intact rocks with different porosity.

When the unloading porosity is calculated the porosity is found using Eq.(9) and used for the pressure calculation in Eq.(7)

3. Model extension for insitu rocks

The presents of joints makes inSitu rock mass weaker. It has been found that both elastic moduli and the unconfined compressive strength decrease for low-qulity rock masses. Numerous empirical equations has been derived for predictions of rock moduli based on parameters defining the quality of rock mass such as RMR,Q,GSI (Sonmez [2006];Singh [2005];Hoek [2002]). We will assume that in-situ-to-intact elastic modulus ratio, F, and the strength reduction factor, SRF, are related as $SRF = F^{\alpha}$. Where α is the coefficient to be found. The values for α suggested by different researchers vary from 0.56,0.72 in Sing [2005] to 2.5 in Sonmez [2006]. One should note, that the joint orientation were not random for the cases considered by the researches mentioned above.

The initial bulk modulus for the in situ rock is matched by enhancing poroelaticity parameter *a* to satisfy the given modulus ratio *F*. In addition to that two main parameters for porous compaction, strain to crush and the compactions slope, are adjusted to match the results of explicit simulations.The model parameters used for the limestone are given in the Table 1.

Table 1 Model parameters for the limestones

Input functions	**Values**	**Description**
$a(\Phi, F)$	$1-\sqrt{F}(1-a_0\sqrt{\Phi})$	poroelasticity function a

a_0	1.3	poroelasticity parameter
$s(F)$	$F^{\alpha/n}, \alpha = 2$	HB scale factor
$m(F)$	$m_i F^{\frac{9\alpha}{28n}}, m_i = 8$	HB parameter
$Y_c(\Phi)$	$0.6exp(-15\Phi)$ GPa	unconfined compressive strength
$Y_t(\Phi)$	$0.01exp(-3\Phi)$ GPa	unconfined tensile strength
C	0.99	$\frac{Y_f}{Y_0}$ ratio
n	0.5	HB power exponent
r	1	power exponent for the cap
$\mu_c(\Phi)$	$\mu_{c0}(\Phi) = 0.005\exp(-15\Phi)$ $\mu_c(\Phi) = \mu_{c0}(\Phi)\frac{1+\xi_1}{F+\xi_1}, \xi_1 = 0.2$	strain to crush
$R_{BD}(\Phi)$	$2exp(-40\Phi) + 0.3$	Brittle-Ductile transition ratio
K_s	81 GPa	solid bulk modulus
ν	0.25	Poisson ratio
$S_0(\Phi)$	$S_{00}(\Phi) = 1 - exp(-8\Phi)$ $S_0(\Phi) = \frac{S_{00}(\Phi)}{1+\xi_2(1-F)}, \xi_2 = 0.4$	compaction slope
D	150	softening rate
ϕ_{cr}	0.001	critical bulking porosity
ε_{hard}	0.06	hardening strain
γ	1.	Gruneisen parameter

$\bar{\gamma}$	0.2	fraction of recompacted bulking porosity
A_1	0.5	degree of associativity at low pressures
A_0	0.5	degree of associativity at high pressures

4. Explicit modeling of jointed rock

Now, when we have a phemenological model with scaling parameters to account for the presence of joints we need some additional information to relate these parameters with characteristics of the joints. Since both intact rock and joints show strongly non-linear response, which is difficult to study analytically we need a numerical model for the jointed rock.

4.1. The joint model

It is know from experimental observations that the joint normal closure is a non-linear function of the applied normal stress resembling a hyperbola (Bandis [1983]). Therefore the normal modulus of the joint, E, can be expressed as

$$E = E_j \frac{a^2}{(a - u_{max})^2} \tag{39}$$

where u_{max} is the maximum joint closure for all times.

The normal force F_n and the shear force F_s are incremented proportionally to the respective moduli E and G as

$$\Delta F_n = A_c E_j \Delta_n / a \quad \Delta F_a = A_c G_j \Delta_s / a \tag{40}$$

where A_c is the area of contact and Δ_n, Δ_s are the normal and the shear displacement increments. The shear forces are limited by the yield surface dependent on the normal force as

$$F_{smax} = \sigma_{coh} A_c + F_n \mu \tag{41}$$

where σ_{coh} is the shear cohesion and μ is the friction coefficient related to the friction angle as $\mu = tan(\varphi)$.

Anytime the yield surface is applied to restrict the shear force, the shear slip u_{sp} is accumulated as

$$\Delta u_{sp} = \frac{\langle | F_s | - F_{smax} \rangle}{G_j A_c} \tag{42}$$

The friction coefficient is changing with the amount of shear slip to account for the softening effects as

$$\mu = \mu_r + (\mu_0 - \mu_r)\langle 1 - \frac{u_{sp}}{u_{sp0}} \rangle \tag{43}$$

where μ_0 and μ_r are the initial and the residual friction angles, and u_{sp0} is the critical shear slip.

To account for joint dilation due to shear slip, the normal forces can be adjusted anytime the shear slip is incremented as

$$\Delta F_n = A_c E \langle 1 - \frac{F_n}{F_{crit}} \rangle tan(\Psi) \Delta u_{sp} \tag{44}$$

where Ψ is the dilation angle and F_{crit} is the critical normal force above which dilation will not occur. The details of the numerical implementation are described in Vorobiev [2007]. The values of the parameters for the joint model used in calculations are listed in the Table 2.

Table 2 Parameters for the joint model

Parameter	**Values**	**Description**
a	0.01 mm	the aperture

E_j	0.5 GPa	normal modulus
G_j	0.5 GPa	shear modulus
Ψ	0	dilation angle
μ_r	atan(30);	residual friction
μ_0	atan(30);	initial friction
σ_{coh}	0.0001 GPa	cohesion shear stress
u_{sp0}	10	critical slip
F_{crit}	$\propto$	critical normal force

4.2. Numerical approach

A generic velocity boundary condition was applied to the boundary nodes of a group of elements. This boundary condition is described by a reference point $\vec{\mathbf{R}}_0$ inside the group and the evolution functions for the components of a symmetric velocity gradient tensor $\mathbf{D}$ Thus the velocity vector for any boundary node was defined as $\vec{\mathbf{V}} = \mathbf{D(t)} \bullet (\vec{\mathbf{R}} - \vec{\mathbf{R}}_0)$ Volume average stress tensor was calculated for the group for each time step. The loading rate was slow enough to ensure quasi-equilibrium conditions. To reduce oscillations due to running waves, static damping was applied. The explicit finite-difference code GEODYN-L was used to update the elements. The joints between the elements were modeled using Simple Common Plane contact algorithm described in Vorobiev [2007].

4.3. Uniaxial compression simulation for a single joint set

To test the method a uniaxial strain compression was appled to a single layer of jointed

elements. Assuming a linear response of the solid and nonlinear hyperbolic stiffening of the joints described by Eq.(39) gives the following relationship between the axial stress, T_A, and the axial strain, ε_A:

$$T_A = \frac{1}{2} E_s \sqrt{\left(\frac{E_j}{E_s} + \frac{a}{d} - \left(1 + \frac{a}{d}\right)\varepsilon_A \right)^2 + 4\frac{E_j}{E_s}\left(1 + \frac{a}{d}\right)\varepsilon_A} - \frac{E_j}{E_s} - \frac{a}{d} + \left(1 + \frac{a}{d}\right)\varepsilon_A \qquad (45)$$

where a is tha aperture, d is the joint spacing, E_j initial joint normal modulus and E_s is the solid modulus. This equation assumes that the deformation is normal to the joint. Figure 5 shows comparison between the analytical expression and the numerical results. For the same joint stiffness, aperture and spacing the numerical results agree with the analytical (dashed curve 1 vs solid line) until the onset of porous compaction not accounted for by the analitical model.

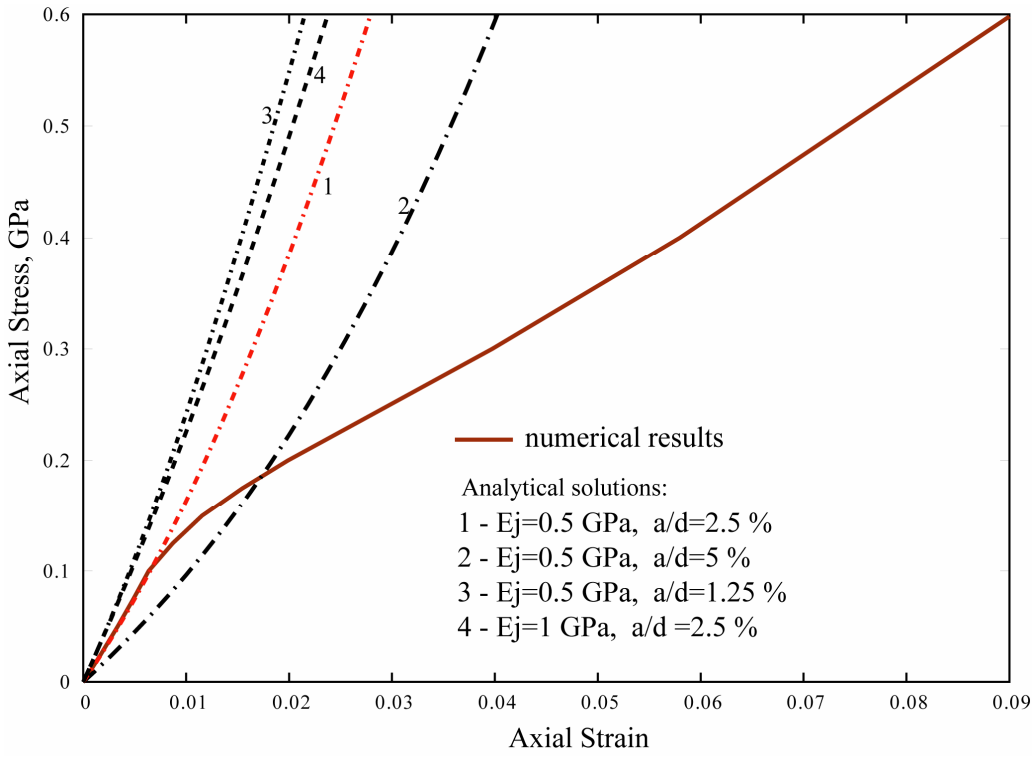

Figure 5 Comparison of the Axial Stress calculated during the uniaxial loading with analytical solutions (dashed lines) for various joint stiffnesses and spacing.

It follows from Eq.(39) that the effective initial modulus is

$$E_0 = E_s E_j \frac{d+a}{E_j d + E_s a} = E_s E_j \frac{1+a/d}{E_j + E_s a/d} \tag{46}$$

The initial modulus is controlled both by the joint stiffness and the ratio of the aperture to the joint spacing, which is the measure of extra porosity introduced by the joints (the joint porosity).

4.4. Simulations of randomly jointed volumes

Since the constitutive model for the InSitu material is isotropic we need to distribute the joints randomly to have an isotropic response for the volume. The following method was used to generate volumes of jointed elements. A cube (volume I) or a sphere (volumes II and III) were meshed using CUBIT meshing tool (Blacker [1994]). Then each element was decoupled from the mesh to represent a block and then subdiscretized into a number of hexahedral elements. Contacts were set between the blocks at the faces of the boundary elements. Resulting angular distributions for the joints were not perfectly random. The least random distribution was found for the sphere with hexahedral blocks. This is because the kernal of the mesh was a cube. The best angular distribution was found for the spherical assembly of tetrahedral blocks (see Figure 7).

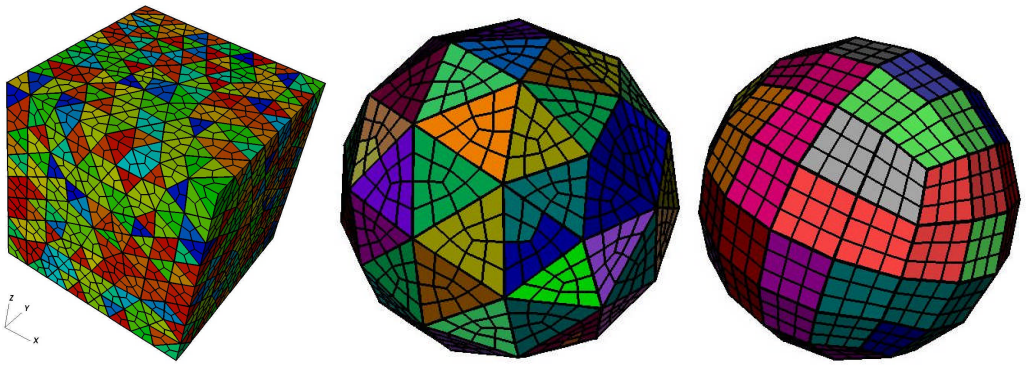

Figure 6 Volumes of jointed elements used in calculations: Volume I-cubical assembly of

tetrahedral blocks subdistretized into hex elements;Volume II -spherical assembly of tetrahedral blocks subdistretized into hex elements; Volume III- spherical assembly of hexahedral blocks subdistretized into smaller hex elements;

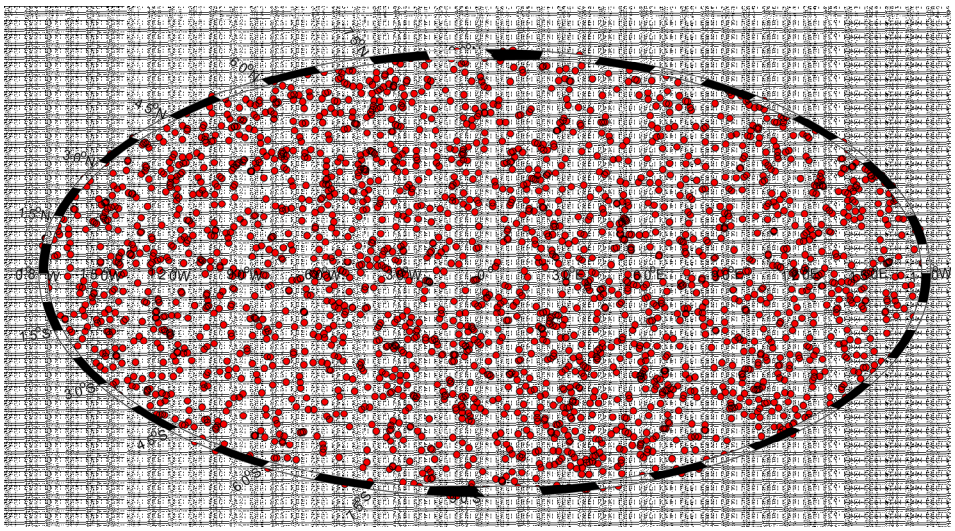

7 Distribution of joints plotted in area preserving Hammer-Aitoff projection for the spherical assemble of hexahedral blocks. Each boundary face is represented as two dots corresponding to the vectors pointing to either side of the face.

To find the constrained modulus for the assembly a uniaxial strain load was applied. The resultant slope between the average stress and the strain gave the effective constrained modulus for the system. Additional biaxial strain loading was applied to find unconfined compressive strength (UCS). The value of UCS was defined at the point of intersection of the uniaxial stress path and the path for the biaxial loading. Figure 8 shows correlations between the calculated constrained modulus ratios and the UCS for various jointed volumes. Each point shown in Figure 8 was defined by two independent runs corresponding to the uniaxial load (to find the modulus ratio) and a biaxial load (to find the ultimate yield surface and UCS) for a particular jointed volume. Proposed correlation function for randomly jointed volumes is shown with a dashed curve. It is known, that the strength of the jointed media depends not only on the joint spacing or the joint properties but also on the persistency of the joints. In the present work this factor was not studied.

Figure 9 shows response of the shperical assembly of tetrahedral blocks in hydrostatic compression. Both loading and unloading paths are shown for various values of the joint aperture.

The less is the aperture the stiffer is the response. Since the joints have a histeresis in load-unload cycles this property is inhereted by the jointed volume. In the current inSitu model this property is not captured since for the elastic deformations loads and unloads follow the same path. The apparent compaction slope changes with increased joint porosity due to increased poroelasticity of the joints. Figure 10 shows comparison of the explicit results with the homogenized model for the hydrostatic compaction.

The modulus ration parameter F was chosen to match the initial bulk modulus to the results of the explicit simulations for the spherical assemble of tetrahedral blocks.

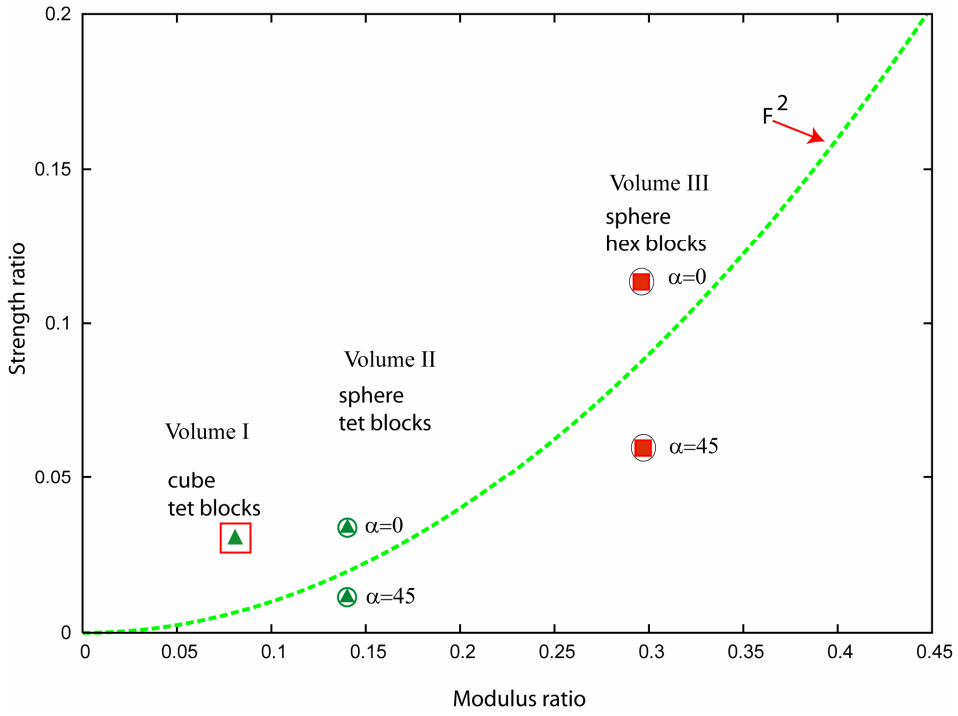

Figure 8. Calculated Unconfined Compressive Strength ratio as a function of the constrained modulus ratio

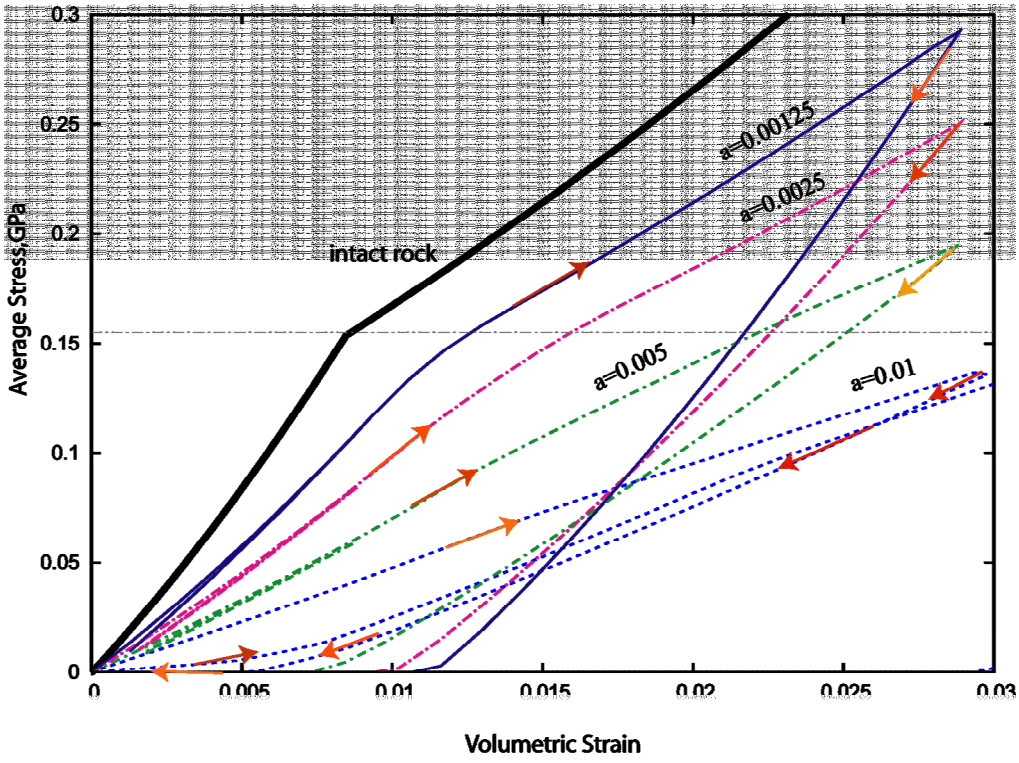

Figure 9 Hydrostatic compression (load – unload) for the spherical assembly of tetrahedral blocks with different joint properties. The bold line shows results for the solid volume (without joints).

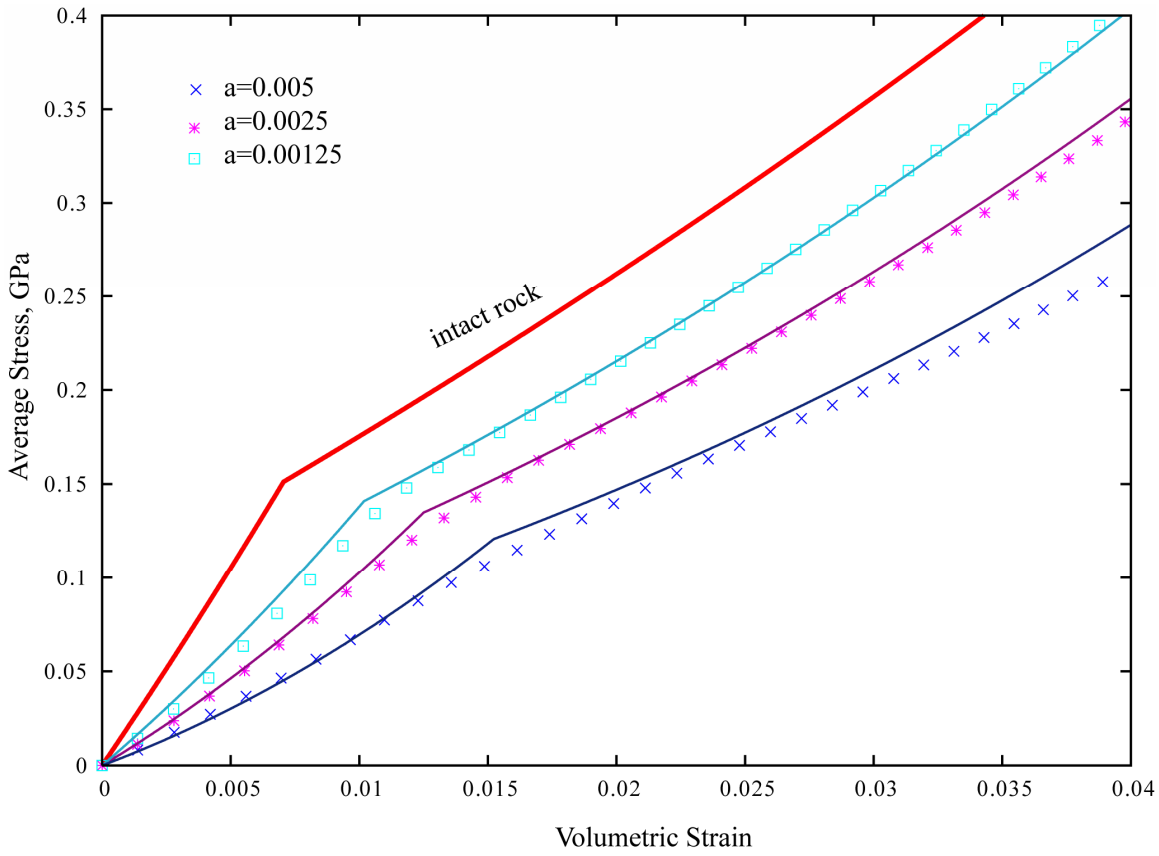

Figure 10 Comparison of the homogenized model (solid lines) with the explicit calculations of hydrostatic compression (markers)

Equation (46) describing effect of a single joint can be generalized for multiple randomly oriented joints as

$$K_0 = K_s E_j \frac{V}{E_j V_s + K_s V_j}, V_j = a\sum A_c \qquad (47)$$

This fomular assumes that the total compressibilty of the volume is a weighted sum of solid and joint compressibilities where the weights are the volumes occupied by the solid and the joints respectively. The volume occupied by the joints is calculated as the product of the joint apperture a and the sum of all contact areas $\sum A_c$. Figure 11 compares the initial part of Pressure-Volume curves generated for hydrostatic compression and the straight lines with the slopes calculated using this formula. It is seen from the picture that for low joint porosities Eq (47) gives desent

predictions for the effective initial bulk modulus. Earlier Fossum [1985] derived the following formula for the average bulk modulus in a randomly jointed elastic media

$$K_0 = \frac{E_s}{9}\left[\frac{3(1+\nu)sE_j/a + 2E_s}{(1+\nu)(1-2\nu)sE_j/a + (1-\nu)E_s}\right] \tag{48}$$

where s is an average joint spacing and ν is the Poisson ratio. In the case of very small joint spacing Eq (48) gives the following limit

$$K_0 = \frac{E_s}{9}\left[\frac{2}{(1-\nu)}\right] = \frac{2K_s(1-2\nu)}{3(1-\nu)} \tag{49}$$

According to Eq (49) the minimum initial bulk modulus depends on the Poisson ratio. For ν=0.35, the solid area between two dotted lines in Figure 11 determins the range of slopes predicted by the formula (48). It is clear that Eq(48) overestimates the bulk modulus if the Poisson ratio remains unchanged. On the other hand there is no recipe given in Fossum [1985] on how to degrade the Poisson ratio for the jointed media.

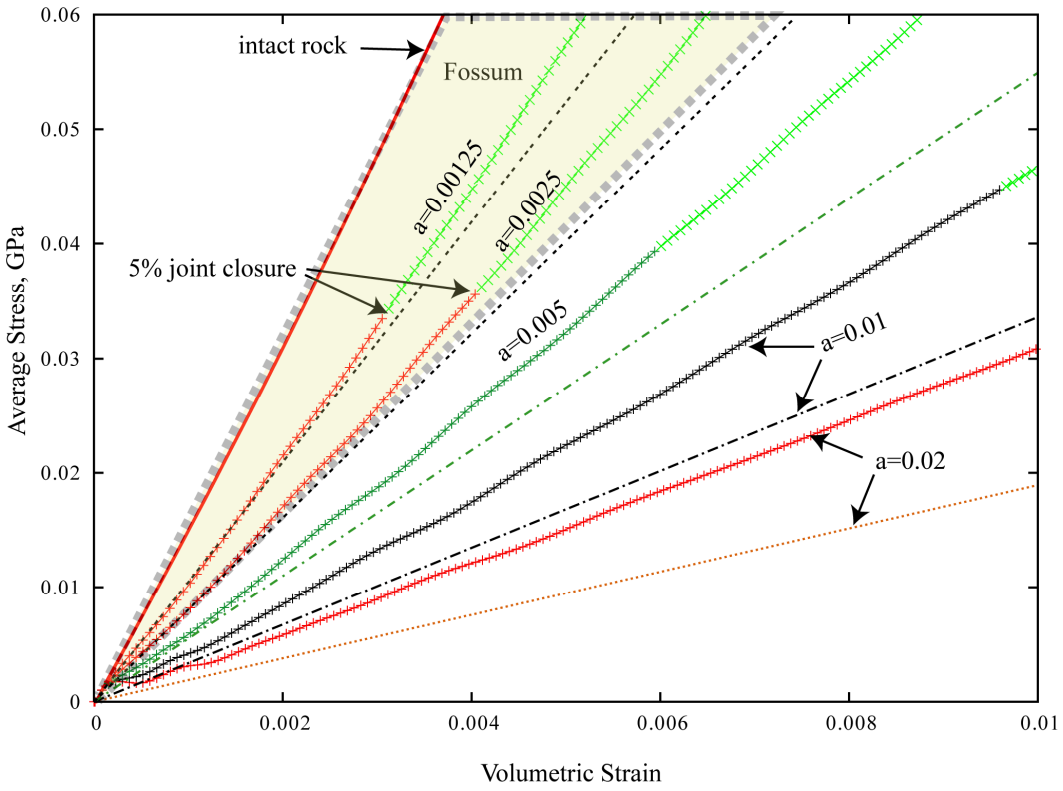

Figure 11 Average stress vs volumetric strain calculated for hydrostatic compression

5. Conclusions

The new parameterized model has been designed for large scale simulations involving rock masses with variable porosity fields and variable GSI index. It is assumed that joints are randomly oriented and the yield surface for the in situ material is found as a scaled yield surface for the intact material. As an alternative to the Hoek-Brown scaling the effective properties of heavily jointed rocks can be found numerically in explicit calculations if both the joint and the solid responses are known.

In many practical cases the joints may have preffered orientations resulting in anisotropic response for the rock mass. To model these cases anisotropic extensions of the current model are nessesary. This is the subject of our future work. The main goal of the present work is to develop thermodynamic framework for homogenized model for jointed rock masses as well as the methodology to derive the key model parameters from the data measured in experiments and

from the explicit simulations.

Acknowledgement

This work was performed under the auspices of the U.S. Department of Energy by University of California, Lawrence Livermore National Laboratory under Contract W-7405-Eng-48.

The author is grateful to colleagues from computational physics group at LLNL: Tarabay Antoun, Joe Morris, Lew Glenn, Ilia Lomov, O.Walton and others.

References

Cundall P.A.,Hart, R.D., 1992, Numerical modeling of discontinua, J.Eng.Computi 9,101-114

Lin,JS, Cheng-Yu,K, 2006, Two-scale modeling of jointed rock masses, Int. Jout. Rock. Mech &Min.Sci 43,426-436

Belytschko, T., Gracie, R.,2007, On XFEM applications to dislocations..., Int. J. Plasticity , doi:10.1016/j.ijplas.2007.03.003

C.S. Desai,M.M. Zaman, J.G. Lightner and H.J. Siriwardane, 1984,Thin-layer element for interfaces and joints, Int.J.Numer. Analyt.Methods Geomech.8,19-43

Wang,J.G., Ichikawa,Y., Leung,C.F., 2003, A constitutive model for rock interfaces and joints, Int.J.Rock Mech.Mng.Sci,40,41-53

Gerrard C.M, 1982,Elastic Models of Rock Masses Having One,Two and Three Stes of Joints, Int.J.Rock Mech.Mng.Sci & Geomech Abstr. 19,15-23

Fossum A.F., 1985, Effective Elastic Properties for a Randomly Jointed Rock Mass, Int.J.Rock.Mech.Min.Sci&Geomech. Abstr., 226,pp.467-470

Cai,M., Horii,H ,1992, A constitutive model of highly jointed rock masses, Mechanics of Materials 13, pp.217-246

Vorobiev O.Yu., 2007, Simple Common Plane contact algorithm for explicit FE/FD

methods, LLNL report, UCRL-TR-227085.

Vorobiev O. Yu., Liu B.T., Lomov I.N., Tarabay T.H., 2007, Simulation of penetration into porous geologic media, Int. Journ. Imp.Engng 34, 721-731.

Aubertin M., Li Li ,2004, Porosity-dependent inelastic criterion for engineering materials, Int.J.of Plasticity 20,2179-2208

Hoek, E., and Brown, E.T.,1998, Empirical Strength Criterion for Rock Masses, Journal of the Geotechnical Engineering Division, American Society of Civil Engineers, 106(GT9), 1013-1035

Cai,M.,Kaiser,P.K.,Tasaka,Y.,Minami,M.,2007,Determination of residual strength parameters of jointed rock masses using the GSI system, Int.Jout.Rock.Mech&Min.Sci 44,247-256

Tiwari,R.P., Rao K.S.,2006, Post failure behaviour of a rock mass under the influence of ... on the true triaxial confinement, Engineering Geology 84,112-129

Pariseau W.G.,1999, An Equivalent Plasticity Theory for jointed rock masses, Int.J.Rock Mech.Mng.Sci, 36,907-918

Rubin M.B., Elata D., Attia A.V., 1996, Modeling added compressibility of porosity and the thermomechanical response of wet porous rock with application to Mt.Helen Tuff, Int.J.Solids Structures 33(6) pp.761-793

Rubin M.B., Vorobiev, O.,Yu., Glenn L.A.,2000, Mechanical and Numerical modeling of a porous elastic-viscoplastic material with tensile failure, Int.Journ.of Solids and Structures,37, pp.1841-1871

S.Y. Xie and J.F. Shao ,2006,Elastoplastic deformation of a porous rock and water interaction, International Journal of Plasticity, 22(12), 2195-2225

Fossum, A.F., and Brannon, R.M.,2004, The Sandia Geomodel. Theory and User's Guide, SAND2004-3226

Shao,J.F , Henry,J.P. ,1991, Development of an elastoplastic model for porous rock,

Int.J.Plasticity, 7,pp1-13

Vajdova V, Baud P., Wong T.F , 2004, Compaction, dilatancy, and failure in porous carbonate rocks ,Journ.Geophysical Research, 109(B05204),1-16

Walsh J.B., 1965, The effect of cracks on the compressibility of rocks, J.Geophys.Res.,70,pp.381-389

Wong,T.,David, C.,Zhu,W ,1997, The transition from brittle faulting to cataclastic flow in porous sandstones:Mechanical deformation,J.Geophys.Res, 102,3009-3025

Mogi,K.,1974, On the pressure dependence of strength of rocks and the Coulomb fracture criterion , Tecnophysics,21,272-285

Baud P.,Schubnel A.,Wong T., 2000, Dilatancy, compaction, and failure mode in Solnhofen limestone, Journ.Geophysical Research,105,B8,pp19289-19303

Chang,C.,Zoback,M.D.,Khaksar,A., 2006,Empirical relations between rock strength and physical properties in sedimentary rocks,Journ.Pet.Sci.Engng.,51,223-237

Torok A, 2006, Influence of fabric on the physical Properties of limestones, in Book: Fracture failure of Natural building stones, Kourkoulis S.K. (ed), 487-497, Springer

Cuss, R.J., Rutter E.H., Holloway R.F.,2003, The application of critical state soil mechanics to the mechanical behaviour of porous sandstones,40,847-862

Vernik,L.,Bruno,M.,Bovberg,C, 1993, Empirical relations between compressive strength and porosity of silicaclastic rocks,Int. Jout. Rock. Mech &Min.Sci.Geomech. Abstr,30,677-680

Sonmez,H.,Gokceoglu,C.,Nefeslioglu,H.A.,Kayabasi,A, 2006, Estimation of rock modulus:For intact rocks with an artificial neural network and for rock masses with new empirical equation,Int. Jout. Rock. Mech &Min.Sci,43,224-235

Singh, M., Rao,K.S.,2005, Empirical methods to estimate the strength of jointed rock masses, Eng.Geology 77,127-137

Hoek,E.,Carranza-Torres,C.t.,Corkum,B.,2002,Hoek-Vrown failure criterion-2002

edition.IN:Proceedings of the fifth North American rock mechanics symposium.Toronto,Canada,1,267-73

Bandis, S.C., Lumsden, A.C.,Barton, N.R.,1983, Fundamentals of Rock Joint Deformation,Int.J.Rock.Mech.Min.,Sci & Geomech.Abstr.,20(6),249-268

Blacker, T.D. ; Bohnhoff, W.J. ; Edwards, T.L., 1994, CUBIT mesh generation environment. Volume 1: Users manual , Sandia Report SAND--94-1100 Sandia National Labs., Albuquerque, NM